ZIBELINE INTERNATIONAL™ PUBLISHING

ISSN: 2576-6724 (Print)
ISSN: 2576-6732 (Online)
CODEN: ACMCCG

Acta Chemica Malaysia (ACMY)

DOI: http://doi.org/10.26480/acmy.01.2025.06.16

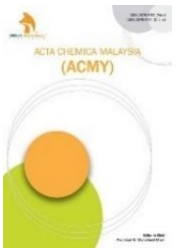

RESEARCH ARTICLE

CARBON QUANTUM DOTS (CQDS) COMPOSITES PHOTOCATALYST FOR PHOTOCATALYTIC DEGRADATION OF WASTEWATER CONTAINING METHYL BLUE DYE

H. M. Solayman[a], Umi Rabiatul Ramzilah P. Remli[a], Md. Arif Hossen[a,b], Kah Hon Leong[c], Sim Lan Ching[d], Noor Yahida Yahya[a], Azrina Abd Aziz[a]*, Minhaj Uddin Monir[e]

[a] Faculty of Civil Engineering Technology, Universiti Malaysia Pahang Al-Sultan Abdullah, 26300 Gambang, Pahang, Malaysia
[b] Center for Environmental Science & Engineering Research, Chittagong University of Engineering and Technology, 4349 Chattogram, Bangladesh
[c] Department of Environmental Engineering, Faculty of Engineering and Green Technology, Universiti Tunku Abdul Rahman, 31900 Kampar, Perak, Malaysia
[d] Department of Chemical Engineering, Lee Kong Chian Faculty of Engineering and Science, Universiti Tunku Abdul Rahman, 43200 Kajang, Selangor, Malaysia
[e] Department of Petroleum and Mining Engineering, Jashore University of Science and Technology, 7408 Jashore, Bangladesh
****Corresponding Author Email: azrinaaziz@umpsa.edu.my***

ARTICLE DETAILS

Article History:

Received 10 December 2024
Revised 5 January 2025
Accepted 10 January 2025
Available online 10 February 2025

ABSTRACT

CQDs are one of the fast growing photocatalyst in the field of nanotechnology due to their excellent chemical, photostability and photoluminescence ability. Recently, CQDs are used as prominence photocatalyst in the field of photocatalytic dye wastewater treatment, bioimaging, bio sensing, bio medicine, photocatalytic hydro production and so on. The purpose of this research is to treat the methyl blue (MB) dye containing wastewater by using CQDs composites derived by water melon rinds (WMR). CQDs, TiO_2, and CQDs/TiO_2 photocatalysts were prepared by hydrothermal method and characterized by XRD, SEM, EDX, BET, XPS, UV-Vis and Photoluminescence spectra. In the results, it is found that CQDs with 0.1 g/L catalyst loading at 5 mg/L of dye concentration has the highest photocatalytic activity with 73% of MB removal compared to TiO_2 (55%) and CQDs/TiO_2 (27%) respectively. The photodegradation rate of MB was decreased with the increased of catalyst loading and higher degradation were achieved at the lowest initial dye concentration. Interestingly the degradation efficiency of MB was increased with augmented of pH concentration. So, this study proved that MB dye is reduced by utilizing CQDs photocatalyst in an environmentally friendly way. Finally, it can be summaries that CQDs has the potentiality to enhance photocatalytic performance.

KEYWORDS

Photocatalytic wastewater treatment, Carbon quantum dots, Methyl blue

1. INTRODUCTION

In recent centuries, world is struggling with handling numerous types of wastewaters generating from household, industry, municipality, and other sources. Wastewater from dye industry is one of them which have direct impact on the environment and human (Al-Thoamy et al., 2022). Around 54%, 21%, 10%, 8%, and 7% of the dye released into the environment each year comes from the textile, dyeing, paper & pulp, tannery & paint, and dye manufacturing industries, respectively (Samsami et al., 2020). Dyes are responsible for water quality loss, interrupt photosynthesis, enhance food chain, promote bioaccumulation and toxicity (Mudhoo et al., 2020). Dye wastewater contains organic pollutants, toxic dyes and heavy metals like chromium, lead, cadmium (Oyeniran et al., 2021; Titchou et al., 2021). To meet the increased human demands, the rate of producing dye wastewater generation is getting higher day by day. Before discharging dye effluent into the environment, appropriate treatment should be implemented using eco-friendly and cost-effective technology.

There are many conventional approaches for the treatment of dye wastewater such as physical (adsorption, ion exchange), chemical (coagulation-flocculation, electrochemical) and biological (enzyme-assisted, bacteria-assisted) (Al-Thohamy et al., 2022; Kurian, 2021). Major drawbacks of these treatment processes include high processing costs, expensive skilled staff, time-consuming procedures, and low processing capacity (Akpomie and Conradie, 2020; Kishor et al., 2021; Liu, 2020). Additionally, these methods may result in secondary pollution by changing colours from a liquid to a solid phase and required additional treatment. In recent times, photocatalysis, an advanced oxidation process (AOP), has been used substantially for the treatment of dye effluent. Photocatalysis has the potentiality to remove and degradation of organic materials, dyes, pesticides, inorganic molecules, microbial pathogens (Ahmad, et al., 2020; Jain et al., 2021). Therefore, in terms of treating dye wastewater, advanced photocatalysis is more suitable, sustainable, and eco-friendly than conventional approaches.

CQDs, a new family of carbon nanomaterials with zero dimensions and sizes smaller than 10 nm is appealing substitutes for semiconductor photocatalysts (Rani et al., 2020). Preparation and synthesis process of CQDs is easy and possible from plant waste, animal waste and industrial waste (Fan et al., 2020). CQDs gained outstanding attraction in several applications such as biomedical, light-emitting devices, bioimaging, and chemical sensing (Rani et al., 2020; Khan et al., 2020). Particularly, CQDs

Quick Response Code	Access this article online	
	Website: www.actachemicamalaysia.com	**DOI:** 10.26480/acmy.01.2025.06.16

Cite the Article: H. M. Solayman, Umi Rabiatul Ramzilah P. Remli, Md. Arif Hossen, Kah Hon Leong, Sim Lan Ching, Noor Yahida Yahya, Azrina Abd Aziz, Minhaj Uddin Monir (2025). Carbon Quantum Dots (Cqds) Composites Photocatalyst for Photocatalytic Degradation of Wastewater Containing Methyl Blue Dye. Acta Chemica Malaysia, 9(1): 06-16.

is widely used in wastewater treatment due to its low toxicity, low-cost, eco-friendly, stable photoluminescence (PL), chemical stability, excellent electron transfer, and electron reservoir features (Rani et al., 2020; Elsayed et al., 2021). CQDs has the ability to adapt to the sun spectrum, improve composite system adsorption capacities, and resist photogenerated electron-hole pairs is becoming increasingly important in photocatalysis (Phang and Tan, 2019).

As a result, CQDs could be high-performance photocatalyst materials, as they emit both down and up-converted PL and expose photo-induced transfer characteristics (Shalahuddin Al Ja'Farawy et al., 2022). Several semiconductor photocatalysts such as TiO_2, g-C_3N_4, ZnO, WO_3 and Fe_2O_3 also used along with CQDs for enhancing the photocatalytic degradation. A group researchers synthesized CQDs with $SrTiO_3$/graphene material for showing the photocatalytic performance and effect of dye degradation (Cui et al., 2022). Some researchers used TiO_2 hybrid composites with CQDs for examining the photocatalytic activity toward dye wastewater degradation (Zhang et al., 2016). On the other hand, TiO_2 is one of the most investigated and advance photocatalyst that offers low cost, lex toxicity, good thermal and optical properties (Shafique et al., 2022). That will potentiality contributing the excellent photocatalytic activity but having major demerits like high electron hole recombination rate.

Herein, we addressed a novel source WMR as a carbon precursor for synthesis CQDs. Also demonstrated a simple hydrothermal process to synthesize CQDs that are anticipated to play a key role in enhancing photocatalytic activity coupling with TiO_2. Subsequently, we analyzed the photocatalytic potentiality of the prepared photocatalysts (CQDs, TiO_2 and CQDs/TiO_2) for the removal of methyl blue dye in the presence of visible light. We also investigated the different environment and dosses of pH, initial dye concentration and photocatalyst dose in the direct and indirect visible light to observe the potentiality of photocatalytic activity.

2. Materials and Methods

2.1 Materials

Fruits waste (watermelon rinds) has been used as a carbon source to extract CQDs. Ethanol (C_2H_6O, 95%), isopropyl alcohol (C_3H_8O, 99.98%), dichloromethane (CH_2Cl_2, 99.8%) titanium (IV) butoxide [$Ti(OBu)_4$), 97.00%], acetone [$(CH_3)_2CO$, 99%], and nitric acid (HNO_3, 99.98%) has been used in this study that are collected from Sigma-Aldrich. All the chemicals were analytical grade and employed straight away without further purification. Distilled water has been applied for the preparation of the sample.

2.2 Synthesis of CQDs, TiO_2 and CQDs/TiO_2

CQDs was synthesized using juice of watermelon rinds and ethanol by hydrothermal process. Collected watermelon rinds were cleaned properly and cut into small pieces before being blended into fine paste using universal blender and filter using 0.1 mm sieve. 30 ml of ethanol and 40 ml of watermelon rinds juice mixture were stirred for five minutes. The mixture was then put into a Teflon-lined stainless-steel autoclave and heated for 150 minutes in an oven at a specific temperature of 120°C. To separate the less fluorescence deposit, the resulting dark brown mixture was rinsed with CH_2Cl_2 and centrifuged at 3000 rpm. To create extremely fluorescent CQDs with sizes in the nano diameter range, excess $(CH_3)_2CO$ is added to the upper portions of the solution and centrifuged at 6,000 rpm.

Titanium (IV) butoxide ($Ti(OC_4H_9)_4$) was used as a precursor to synthesize TiO_2 solution via partial analysis and poly-condensation with water (H_2O). Nitric acid (HNO_3) was used as catalyst to enhance hydrolysis and isopropyl alcohol $(CH_3)_2CHOH$ as the solvent. The $Ti(OC_4H_9)_4$: H_2O with the mole ratio 1: 2 was prepared approximately. Then, the mixture was stirred vigorously by a magnetic stirrer for more than one hour. Finally, the resulted transparent colored solution was calcined in a muffle furnace for an hour at 500 °C. In order to synthesis CQDs-based nanocomposite, 0.3g of prepared TiO_2 was dissolved at room temperature in the CQDs solution. The solution was then transferred into Teflon-lined-stainless-steel autoclave and heated at 120 °C for 3 hours. The final product was collected by centrifugation, washed with deionized water several times to remove the impurities and finally dried in room temperature for a day.

2.3 Characterization

The crystal structure of prepared powders was characterized by an X-ray diffractometer (XRD, PANALYTICAL, X'PERT3 POWDER). The scans were performed in the range of 2θ range between 10^0 to 80^0 with 0.02^0 step size and 1s step time. The morphologies of samples were examined by scanning electron microscope (SEM) and energy dispersive X-ray spectroscope (EDX) (Hitachi Model, TM3030 Plus). The samples were acquired at 30 seconds acquisition time with 15 kV of accelerating voltage. High-resolution transmission electron microscopy (TEM, TECNAI, G2 20 LaB6) was utilized to observe the geometric morphology and particle size of the synthesized samples. The prepared photocatalysts' surface area, pore diameter, and pore volume were evaluated by Brunauer-Emmett-Teller (BET, MICROMERITICS, ASAP2020). Chemical state and chemical composition analysis was carried out using X-ray photoelectron spectroscopy (XPS, ULVAC-PHI 5000, VersaProbe II) with a beam current of 15 mA and operating voltage of 12 kV. The optical absorption range and the band gap energy were measured by UV–visible spectrophotometer (UV–Vis, SHIMADZU) and Photoluminescence spectroscopy (PL, EDINBURG INSTRUMENTS, F900).

2.4 Photodegradation of MB

A self-assembled reactor equipped with a 500 W Halogen lamp (<420 nm) UV cut-off filter was used to perform the photocatalytic activity. Entire photoreactor was fully covered with aluminum foil to prevent external light from interfering the photocatalysis reaction. To ensure the degradation of MB, two sets of control experiments (adsorption and photolysis) were carried out. 5g of photocatalyst was added to 150 mL of MB solution for the adsorption experiment magnetically stirred at 500 rpm in the dark for 2 hours at room temperature. 150 mL of MB solution was placed in the reactor under artificial light without the presence of photocatalyst for photolysis experiment.

After completing the control experiments, 150 mL of MB solution was filled in 500 mL beaker as reaction vessel at room temperature. Prior to the irradiation, a specified amount of as-prepared CQDs, TiO_2 and CQDs/TiO_2 was dissolved in MB solution. These mixtures were kept under magnetic stirring at 500 rpm for 30 min, corresponding to the time needed to establish the adsorption/desorption equilibrium at room temperature. Afterwards, 500 W halogen lamp was switch on and positioned above 11 cm from the surface of reaction of solution. The reaction was performed for 120 min and the solutions were collected for every 20 min. There are three parameters studied for the degradation of MB which is effect of catalyst loading, effect of initial concentration of MB solution and pH of MB solution. The photocatalyst loading was varied at 0.1 g/L, 0.2 g/L, 0.3 g/L, 0.4 g/L and 0.5 g/L. The initial concentration of dye (MB) solution was used at 5 mg/L, 10 mg/L and 15 mg/L and pH level was 3.00, 7.00 and 9.00 that balanced by using H_2SO_4 and or NaOH solutions. The degradation rate of dyes can be calculated by using the following equation:

$$\text{Degradation rate} = \frac{C_0 - C}{C_0} \times 100\% \quad (1)$$

Where, C_0 = initial concentration of MB, C = final concentration of MB

3. Results and Discussion

3.1 Characterization of CQDs, TiO_2, and CQDs/TiO_2 composite

3.1.1 XRD

The crystal structure of CQDs, TiO_2, and CQDs/TiO_2 was revealed via a powder X-ray diffraction investigation presented in Figure 1. The XRD pattern of CQDs shows a broad diffraction peak at about 2θ = 29.31° corresponds to (002) lattice plane. No peak found for CQDs in XRD due to the amorphous form, closely packed carbon atoms with alkyl groups and very low amount (Shafique et al., 2022). This finding shows consistency with previous studies that demonstrated similar peak (Kumar et al., 2017; Liu et al., 2017). On the other hands, TiO_2 exhibits four different peaks at 27.63°, 36.29°, 41.44° and 56.81° which attributed to (110), (101), (111) and (220) facets of rutile TiO_2 that also concur with the XRD pattern obtained in previous studies (Haque et al., 2017; Sugapriya et al., 2013). The modified CQDs/TiO_2 composite shows XRD peaks at 28.27°, 34.19°, 40.63° and 58.75° which are slightly different with the pure TiO_2. The peaks value is observed to be slightly shifted due to the incorporation of CQDs that could have caused the lattice relaxation within the composite (Hou et al., 2019).

According to the crystal structure in XRD, TiO_2 is appears in CQDs/TiO_2 composites where their patterns are closely similar due to high dispersion, small amount and low crystallinity of CQDs. The XRD pattern revealed the TiO_2 possessed with a tetragonal crystal structure. The TiO_2 crystallite size was estimated to be 45.55 nm using Scherrer's equation adopting the strongest peak of the pure rutile phase, hence indicating TiO_2 powder consist of highly crystalline nanoparticles with larger crystallite size compared to anatase phase (Haque et al., 2017). In addition, crystallite size of CQDs/TiO_2 was estimated to be 45.91 nm using Scherrer's equation and this result was in good agreement with the TEM study. CQDs and CQDs/TiO_2 are in uniform size based on their dimensions. We also noticed slight reduction of particle size that led to increase the photocatalyst surface area that enhanced the interaction between photons and atoms.

Finally, contributed to increase the rate of photocatalytic dye treatment by producing more effective species.

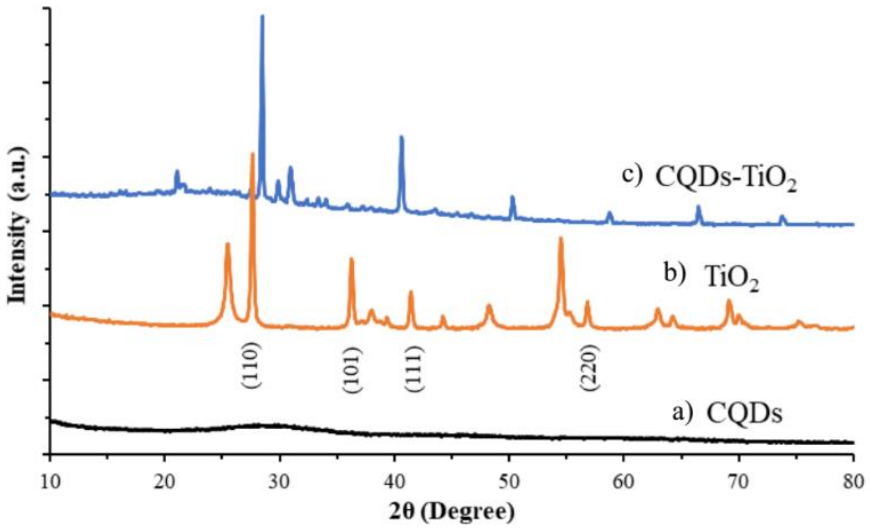

Figure 1: XRD pattern of (a) CQDs, (b) TiO_2, and (c) CQDs/TiO_2 composite

3.1.2 SEM + EDX

Figure 2 (a,b,c) shows the SEM analysis that conducted to examine the surface morphology of CQDs, TiO_2 and CQDs/TiO_2 photocatalysts. As depicted in Figure 2a, synthesized CQDs shows irregular porous shapes of nanostructured. This can be the result of the poor dispersion of CQDs in water during the preparation procedure and subsequent aggregation from long-term storage prior to analysis. Figure 2b demonstrated that TiO_2 comprises uniform nanostructure of spherical shapes particles with small amount of agglomerated structure due to the high calcination temperature. In general, the structure of TiO_2 is very sensitive to the calcination temperature in which high calcination temperature would cause the fine particles to be grown in larger size and agglomerate to form larger particles size [26]. On the other hand, CQDs/TiO_2 composite were found almost spherical shape and it is hard to get the accurate morphology of CQDs/TiO_2 (Shafique et al., 2022).

Figure 2 (d,e,f) states the EDX spectrum was conduct for determining the element compositions of CQDs, TiO_2 and CQDs/TiO_2. The EDX spectrum of CQDs unveils the C, O, Na, K, Cl and Au elements presence in CQDs as depicted in Figure 2d. The CQDs comprises mainly of C (51.57 wt.%) and O (34.50 wt.%) that possibly due to the presence of oxygenated surface functional groups such as carboxyl and hydroxyl. Since CQDs was derived from biomass (watermelon rinds) that generally contains of carbon, hydrogen, and oxygen (Olatunji, 2019). In the EDX spectrum of TiO_2, the existence of Ti, O and C and elements were observed as depicted in Figure 2e. The contents of Ti and O detected were 44.57 wt.% and 43.95 wt.% respectively which was similar to the previous study that employed the same preparation method (Juliet et al., 2017). EDX spectrum of CQDs/TiO_2 specifically remarked the existence of Ti, O, C, Si, K and Au with Ti (36.96 wt.%), O (32.76 wt.%) and C (10.55 wt.%) as the major elements (Figure 2f). It is assumed that an adjustment on the components would affect the production of surface defect sites which could have impacted to the photocatalytic performance (Ke et al., 2017). However, more studies need to be conducted in the future to rectify the above postulation.

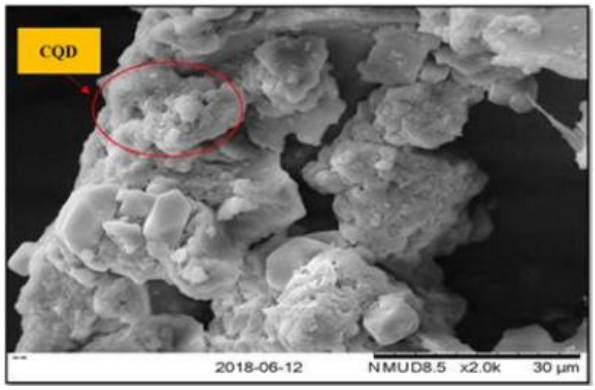

a

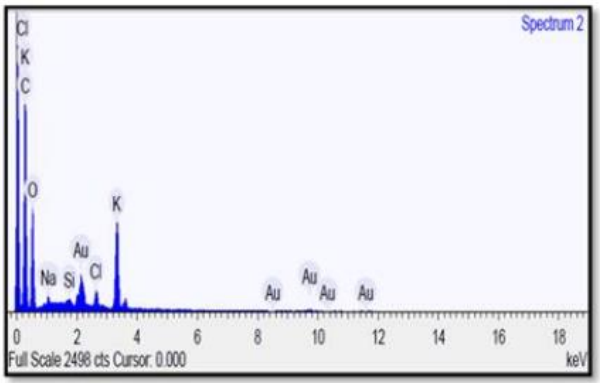

d

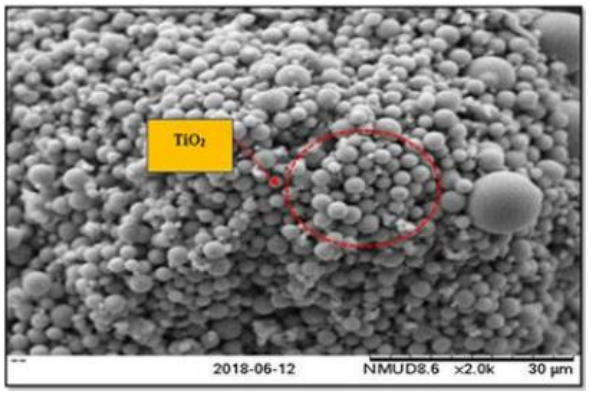

b

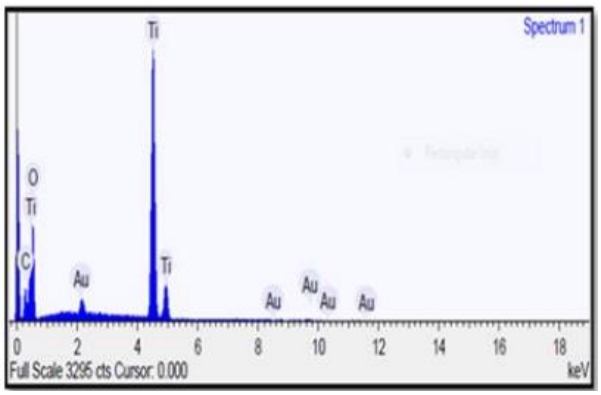

e

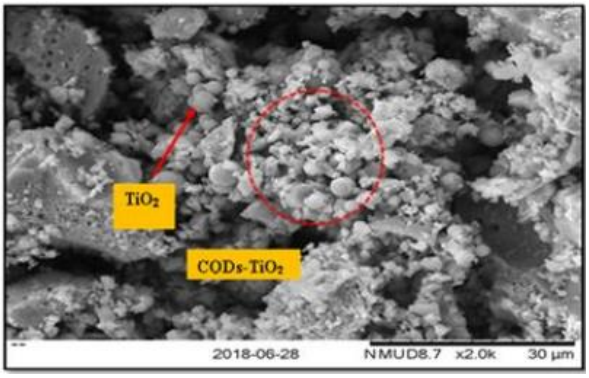

c

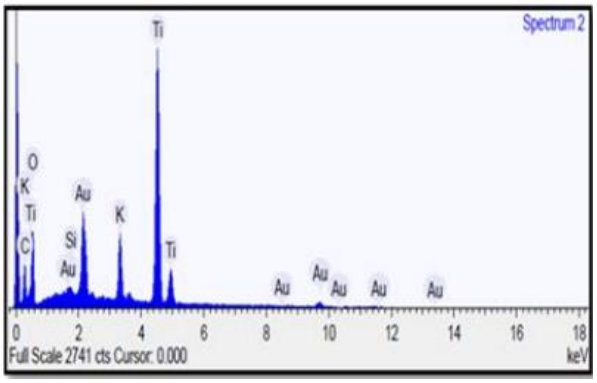

f

Figure 2: SEM image: a) CQDs, b) TiO_2, c) CQDs/TiO_2 and EDX spectrum: d) CQDs, e) TiO_2, f) CQDs/TiO_2

3.1.3 TEM

Figure 3, shows the TEM image of CQDs, TiO_2 and CQDs/TiO_2. As depicted in Figure 3a, a band of spherical dots was observed on CQDs which revealed that the particles were completely dispersed in water and well separated among each other. The spherical morphology was clearly visible with narrow size distribution ranging from 3.18 to 4.67 nm. The size of the CQDs produced was comparable to the previous studies conducted (Ke et al., (2017). TEM analysis of TiO_2 revealed that the cluster's structure was formed due to the agglomeration of TiO_2 particles as shown in the SEM image (Figure 2b). The clusters mainly composed of spherical morphology with average crystallite size around 45.55 nm (Figure 3b) that was calculated using Scherrer equation. Figure 3c, shows the TEM image of CQDs/ TiO_2 composite with 45.91 nm in size which is slightly bigger than TiO_2. The dark speckles in the TEM images of CQDs/TiO_2 composites addressed the existence of CQDs on the surface of the TiO_2. Additionally, it was discovered in this study that the preparation of CQDs under mild conditions led to the conceivable formation of finer particles with a narrow size distribution.

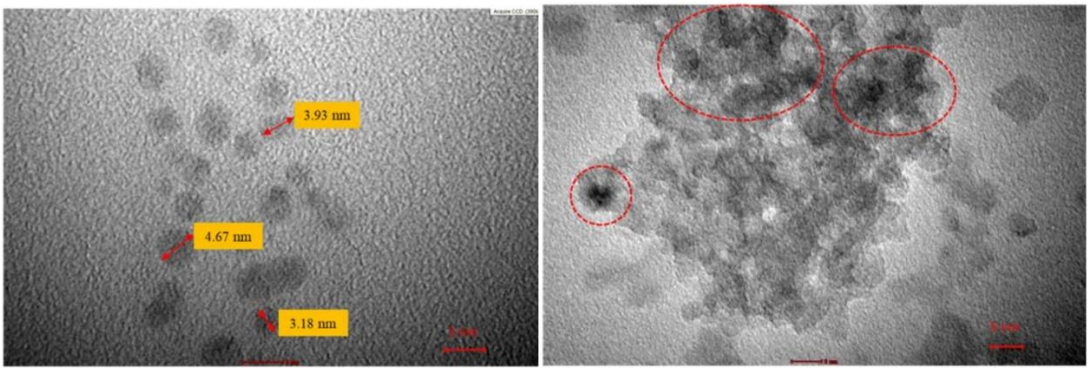

a b

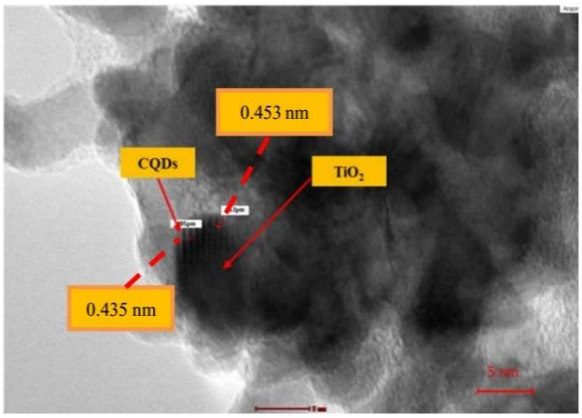

c

Figure 3: TEM image of a) CQDs, b) TiO_2, and c) CQDs-TiO_2

3.1.4 XPS

The chemical nature of interaction between the CQDs and TiO_2 was investigated by X-ray photoelectron spectroscopy (XPS). Figure 4, shows the elemental analysis for XPS spectra of carbon (C 1s), titanium (Ti 2p) and oxygen (O 1s) in the CQDs/TiO_2 composite. Figure 4a, shows the XPS spectrum of CQDs/TiO_2 composite. As depicted in Figure 4b, C 1s spectrum of CQDs was divided into three peaks (i.e., 283.7 eV, 284.9 eV, 286.9 eV) that can be attributed to the sp2 carbon, C-C bond, and C-O-C bond respectively in which the findings obtained were comparable with previous study (Ke et al., 2017). Figure 4d, deconvolutes the O 1s peaks at 528.9 eV, 530.0 eV and 531.7 eV that can be assigned to Ti-O, C-O and C=O bond respectively. Furthermore, the Ti 2p spectra detected (Figure 4c) with two obvious peaks at 458.0 eV and 464.0 eV that can be ascribed to the Ti 2p 3/2 and Ti 2p ½ of TiO_2. Additionally, no peak was observed for Ti-C bond in the CQDs/TiO_2 composite which indicated that the CQDs does not exist as a dopant in the composite and thus the development of new bond between CQDs/TiO_2 can be ruled out (Ke et al., 2017). Overall, it can be concluded that the CQDs/TiO_2 heterojunction composites were firmly shaped via electrostatic interaction between the CQDs and TiO_2, which could subsequently empower the photoexcited-charge transporters to exchange through the contact interface.

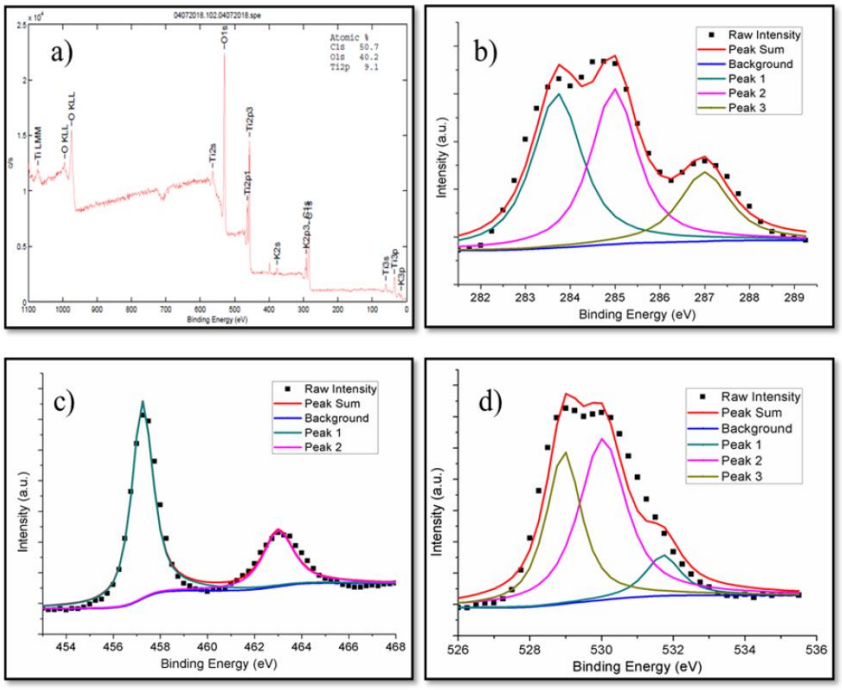

Figure 4: The XPS spectra of a) CQDs/TiO_2, b) C 1s, c) Ti 2p and d) O 1s

3.1.5 UV-Vis and Band Gap Energy

Figure 5 and Figure 6 shows the UV-Vis spectrum and band gap energy of CQDs, TiO_2 and CQDs/TiO_2 respectively. The UV-Vis absorption spectrum of CQDs solution performed in the range of 300 nm to 900 nm was exhibited in the Figure 5a. Only one intense absorption peak was observed in the UV region at about 317 nm which can be correlated to n- π* transitions of C=O bonds in CQDs with a tail elongating to the visible range (Wang and Hu, 2014). Hence this optical characteristic will lead to bandgap narrowing on the semiconductor as a result CQDs can extend the light absorption range in enhancing the photocatalytic degradation. Figure 5b, shows the UV-Vis absorption spectrum of TiO_2 where the significant absorbance that recorded at the wavelength 405 nm could be attributed to the light absorption that aroused by the excitation of electron from valence band to the conduction band (Wang et al., 2012). UV-Vis analysis of CQDs/TiO_2 observed one intense peak (315 nm) in the UV region and tailing into visible light region as shown in Figure 5c. The peak value of CQDs described the distinctive adsorption pattern which was also reported (Zhang et al., 2016). Finally, due to the peak range it is proved that there is an enhancement of absorption in the visible region. Roughly spherical and typically unique optical characteristics makes CQDs as a promising applicable catalyst.

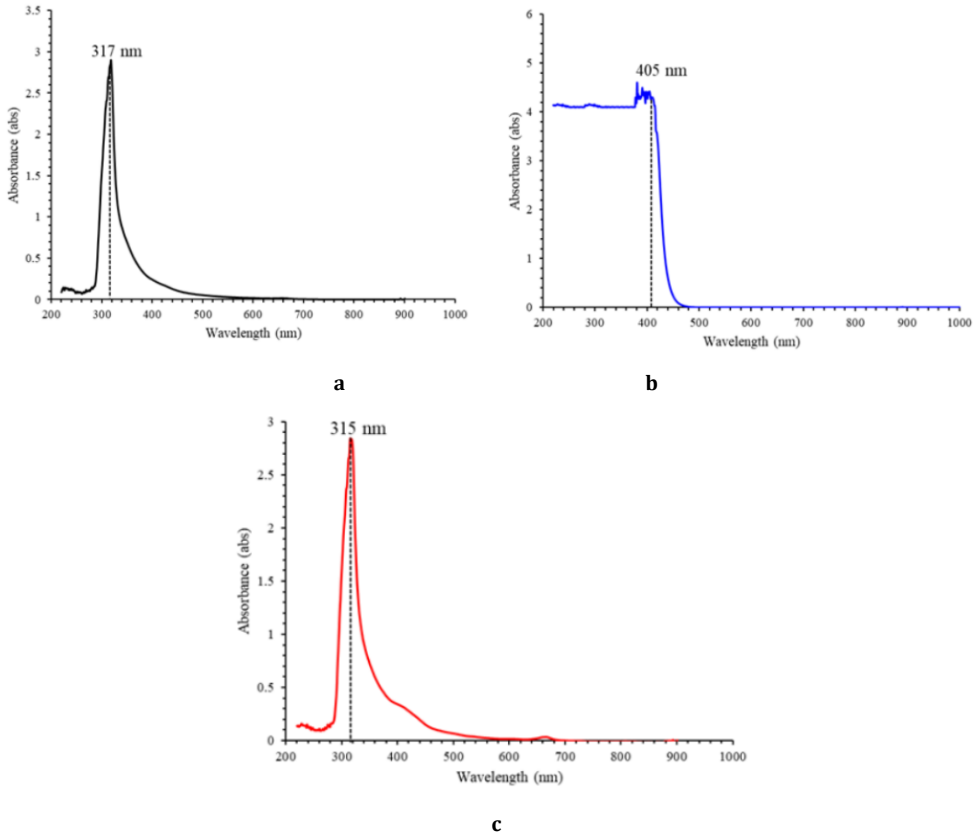

Figure 5: The UV-Vis spectrum of a) CQDs, b) TiO_2, and c) CQDs/TiO_2

Figure 6 (a,b,c), shows the bandgap energy of CQDs, TiO_2, and CQDs/ TiO_2 where the value has been found at 3.73 eV, 3.42 eV and 1.57 eV, respectively. The decreasing of band gap value from 3.73 to 1.57 eV of each catalysts suggested that photons are present in visible area and improved

the photocatalytic performance (Shafique et al., 2022; Singh et al., 2018). The band gap value obtained was higher compared to the band gap value of crystalline phase reported in the previous study (Valencia et al., 2010). The behavior and differences in bandgap values of rutile phase can be attributed to the crystalline size of the catalysts which are in agreement with the XRD result. During the hydrolysis, both Ti (OH)4 and 4R(OH) have been successfully resulted from the reaction between Ti (OR)4 and 4H2O with lower water molar ratios than the stoichiometric. However, a large quantity of non-hydrolyzed alkoxy anions were resulted from the incomplete hydrolysis reaction and subsequently absorbed onto the surface of TiO2. This explains the formation of less crystalline TiO_2 with irregular shapes and uneven distribution of particle sizes that lead to low surface area (Valencia et al., 2010).

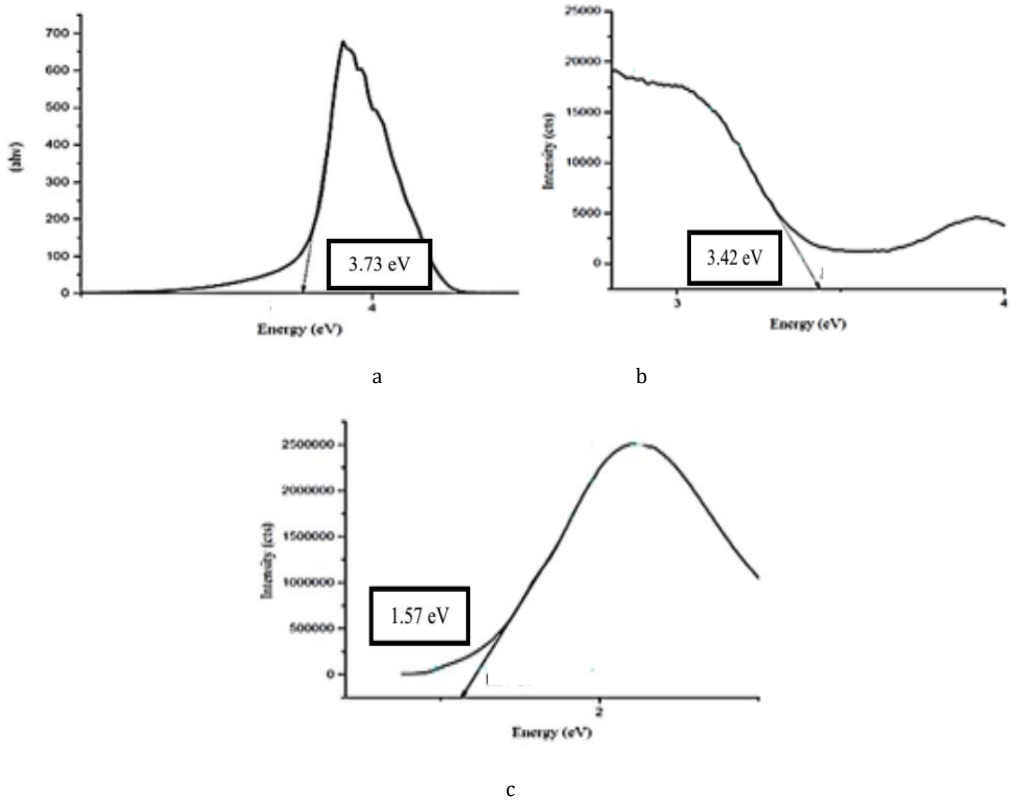

Figure 6: The band gap energy of a) CQDs, b) TiO_2, and c) CQDs/TiO_2

3.1.6 BET

The porosity and surface area of the catalysts were determined using the N2-adsorption-desorption isotherm and the particles size was estimated using Scherrer Equation. Table 1 summarizes the porous characteristic of CQDs, TiO_2 and CQDs/TiO_2 including BET surface area, pore volume, pore width and particle size. BET surface area, pore volume, pore width and particle size of CQDs, TiO_2, and CQDs/TiO_2 was recorded as 676.38, 38.86 and 39.53 m^2/g; 0.54, 0.24 and 0.21 cm^3/g; 34.83, 245.85 and 212.20 Å; 10.12, 45.55 and 45.91 nm, respectively. It should be mentioned that the BET surface area and pore volume of CQDs obtained were higher than the one produced from waste car bumper (120.3 m^2/g, 0.125 cm^3/g, respectively), indicating watermelon rinds could be a promising feedstock for CQDs preparation (Mohamed and Alsanea, 2020). Though CQDs was observed as smaller particles and pore width also low in BET analysis that also found in the TEM analysis. Smaller particles size can provide more active sites for adsorption of pollutants onto the surface of catalyst (Zhang et al., 2016). That can contribute to increase the photocatalytic activity of CQDs. The higher pore volume possesses by the CQDs can cause rapid diffusion of organic pollutants during the photocatalytic process. All of these above results addressed the enhancing capacity of BET surface area.

Table 1: Porous characteristic of CQDs, TiO_2, and CQDs/TiO_2

Photocatalyst	CQDs	TiO_2	CQDs/TiO_2
BET surface area (m^2/g)	676.38	38.86	39.53
Pore volume (cm^3/g)	0.54	0.24	0.21
Pore width (Å)	34.83	245.85	212.20
Particle size (nm)*	10.12	45.55	45.91

*Note: *Estimated using Scherrer Equation*

3.1.7 PL

PL emission spectra were investigated to determine the separation efficiency of the charge carrier of the samples prepared. Figure 7 (a,b,c), shows the PL spectrum for CQDs, TiO_2 and CQDs/TiO_2. Figure 7a, illustrates the PL emission spectra behavior of CQDs across the excitation wavelength at 360 nm. The PL emission spectra of TiO_2 (Figure 7b) shows that the emission intensities produced a broad emission band due to the agglomerated lattice sites. It was observed that the shape of the PL spectrum widened and split into several peaks at 315 nm, 412 nm, 464 nm, 675 nm, and 820 nm. The sharp peak observed at 315 nm shows a strong absorption in UV region which may originate from the charge transfer response of TiO_2 from valence band (VB) to the conduction band (CB). The peak shift towards red wavelength may have induced by the large particle size of TiO_2. Overall, the results indicated that the PL intensity was slightly reduced thus reduced the recombination rate (Haque et al., 2017).

The PL emission spectra of CQDs/TiO_2 exhibits a wide signal in the range of 450 nm to 850 nm (Figure 7c), which is within the range of visible light. Similar observation was reported by a group researchers in which the author claimed that the incorporation of TiO_2 on the CQDs may have increased the surface electron charge of the TiO_2 (Yan et al., 2019). And this subsequently amended the basic process of electron-hole pair formation of the CQDs/TiO_2 under visible light radiation. The maximum PL peak was detected at 585 nm for both CQDs and CQDs/TiO_2 which could be attributed to the excitonic PL that mainly resulted from the surface vacancies of oxygen and interface traps of radiative defects in the boundaries between carbon and TiO_2. The incorporation of CQDs enhance the electron charge transfer by reduce the recombination rate and remaining the peak of CQDs/TiO_2 in PL analysis under visible light. Large spectral width of the observed PL band is caused by inhomogeneous broadening due to a variation in particle size.

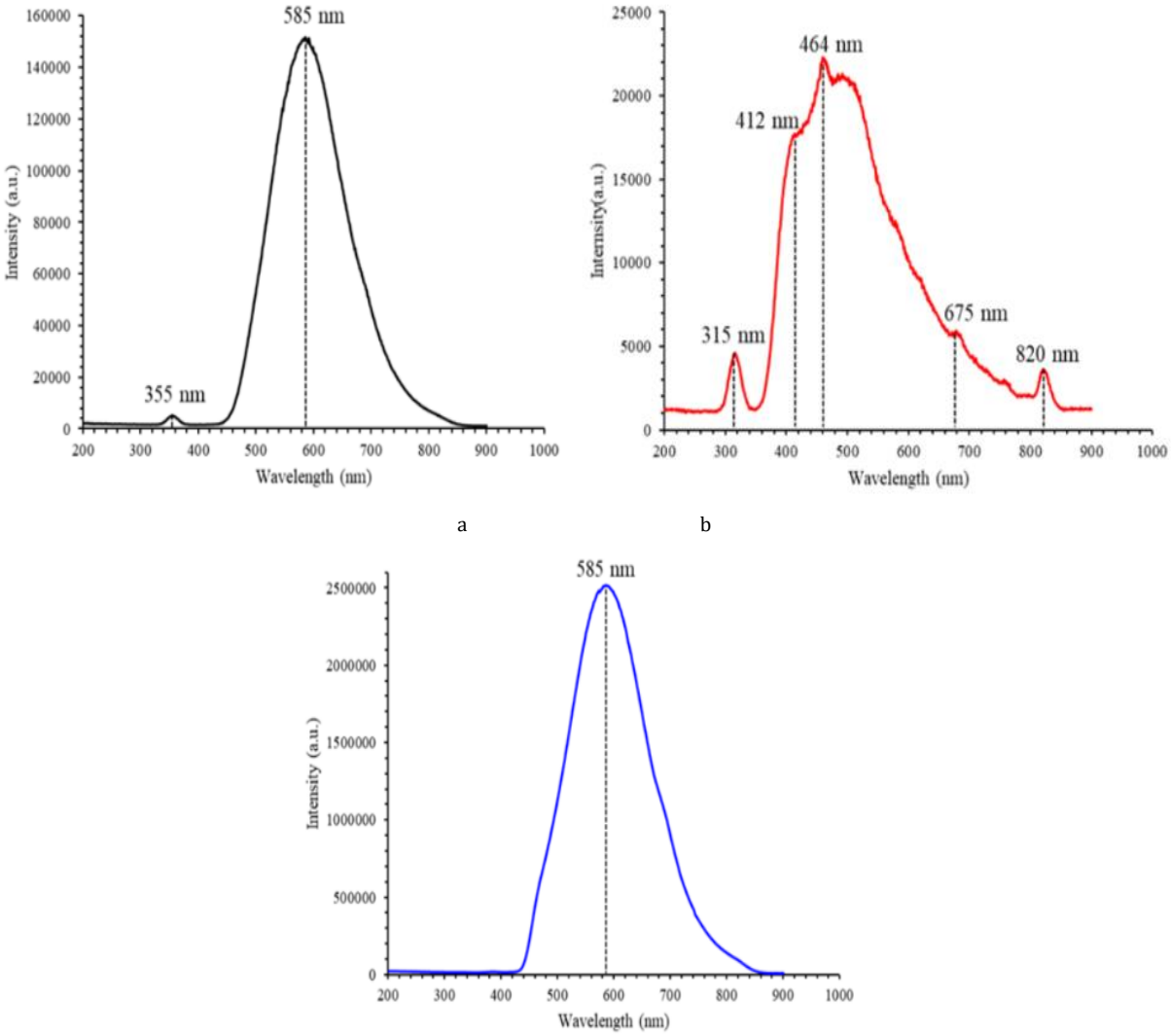

Figure 7: The PL spectrum of a) CQDs, b) TiO_2, and c) CQDs/TiO_2

3.2 Evolution of photocatalytic performance

3.2.1 Control experiments

Control experiments (adsorption and photolysis) were carried out to make sure that the MB is degraded due to photocatalytic activities and UV light has the potentiality to degreed the organic compounds in the absence of photocatalyst. Figure 8 (a,b,c), depict the adsorption process employing CQDs, TiO_2, and CQDs/TiO_2 after 30 minutes degradation was around 16%, 7%, and 8%, respectively. The effect of adsorption can be considered negligible because the degradation is insignificant, implying that it plays a modest role in the MB elimination mechanism. Therefore, photolysis will not be able to degrade MB on its own (Figure 8d).

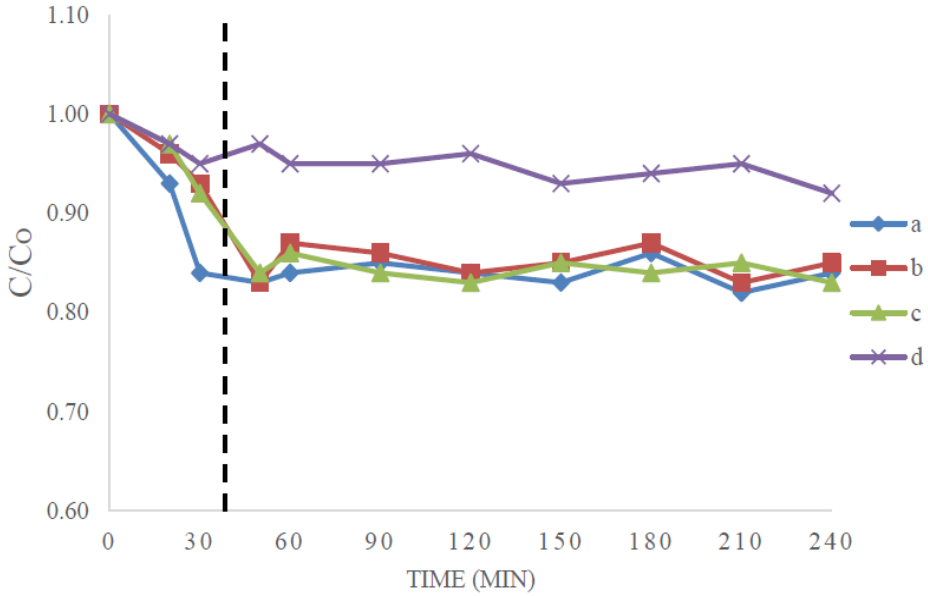

Figure 8: Controls experiments a) adsorption of CQDs, b) adsorption of TiO_2, c) adsorption of CQDs/TiO_2 and d) photolysis of MB

3.2.2 Effect of catalyst loading

The photodegradation rate of MB was decreased with the increased of catalyst loading as showed in Figure 9. This may be due to the aggregations of the catalyst particles which prompted to the decreasing number of actives site for binding of MB molecules on the catalyst for subsequent degradation reaction (Ke et al., 2017; Jawad et al., 2018). CQDs recorded the highest MB degradation ability as depicted in Figure 9a. This could be due to the smaller particles size and higher BET surface area of CQDs. Hence, the percentage of degradation of TiO_2 took the lowest value (35%) among the other catalyst Figure 9b. As showed in Figure 9c, a lower MB degradation percentage (27%) of CQDs/TiO_2 was recorded to be lower than CQDs. This may be caused by the existence of rutile phase of the TiO_2 on the CQDs/TiO_2 composite. It was reported that, the rutile phase of TiO_2 is less reactive than anatase phase in terms of photocatalytic activity (Yan et al., 2019).

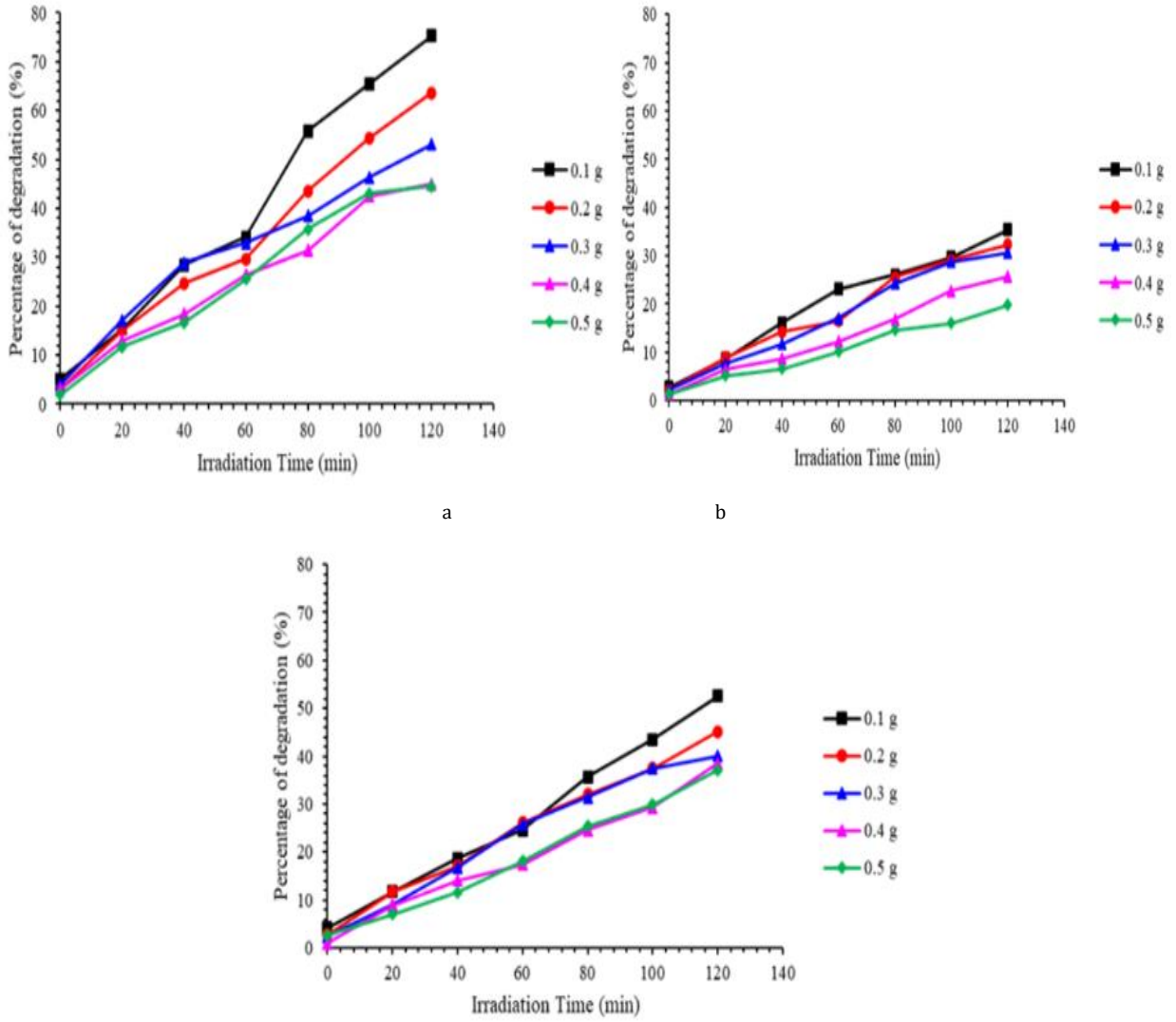

Figure 9: Effect of catalyst a) CQDs, b) TiO_2, and c) CQDs/TiO_2 loading on photodegradation of MB

3.2.3 Effect of pH

Table 2 presents the percentage degradation of MB under the influence of different pH conditions (i.e., acidic, neutral, and alkali) ranging from 23.1–81.0%. CQDs shows the highest degradation percentage at the pH of 9 while TiO_2 recorded with the lowest value at pH 3. It was found that CQDs performed as the best photocatalyst in MB degradation compared with TiO_2 and CQDs/TiO_2 regardless of the pH conditions. In addition, the results also inferred that alkali condition is more favorable for MB degradation since higher percentage degradation was obtained at higher pH regardless of the photocatalyst used. This could be due to the electrostatic interaction between the negative surface functional group of the photocatalysts and the MB dye with positive charge (Lima et al., 2019; Jiaqi et al., 2019).

Table 2: Percentage degradation of MB under different pH conditions

pH value	Percentage degradation of MB (%)		
	CQDs	TiO_2	CQDs/TiO_2
3.0	44.3	23.1	34.4
7.0	69.4	26.8	45.8
9.0	81.0	32.1	50.1

3.2.4 Effect of initial dye concentration

Figure 10 (a,b,c) shows the effect of initial dye concentration (5, 10 and 15 mg/L) for the degradation of methylene blue with CQDs, TiO_2 and CQDs/TiO_2 catalysts. In general, higher degradation percentage were achieved at the lowest initial concentration (5 mg/L) and decreased when the initial concentration was increased from 5 mg/L to 15 mg/L. This could be due to the concentration of MB have exceeded the limit for which the free radicals generated on the surface of the catalysts can be degraded. On the other hand, it is reported that a longer reaction time is required to fully degrade the high concentration of MB solution (Tharaneedhar et al.,

2017). So, it concludes that the dye concentration is significantly influence the dye degradation performance.

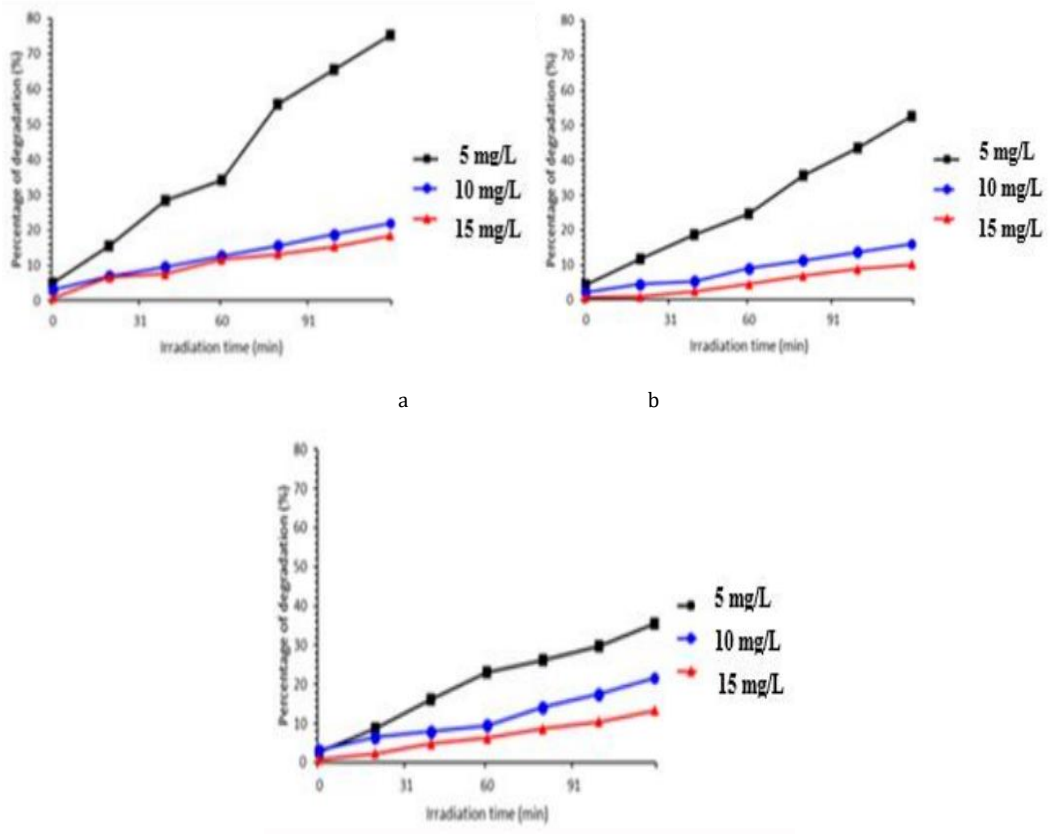

Figure 10: Initial concentration of a) CQDs b) TiO_2 c) CQDs/TiO_2 for MB degradation

Figure 11 shows the MB dye degradation mechanism by CQDs/TiO_2 composite where TiO_2 deposited on CQDs catalyst. Dye molecules are adsorbed by the CQDs/TiO_2 composite surface where the photocatalytic reaction occurs. When light energy adsorbed by MB, electron was excided from conduction band (CB) of TiO_2 to valance band (VB) and transformed MB^{+}• which is crucial for additional photocatalytic reaction. The excited MB^{+} energy level was overhead the CB of TiO_2, which would have served as an impetus for electron inoculation. The excited electron reacted with oxygenated compound on the surface of CQD to form radical compounds. This radical compound then be reacted with MB and formed degraded products. Only a minority of the charges might take part in the photocatalytic reaction since these electrons quickly recombine with other ions.

When CQDs/TiO_2 composite formed by depositing CQDs on TiO_2 then the electron on CB of TiO_2 aimed to transfer on CQDs. The CQDs facilitated electron transport, which led to effective electron MB^{+} pair separation and increased photocatalytic activity. Oxygen in the solution then react with an electron on the CQDs to produce O2 that plays a significant part in photodegradation, which results in impressive photocatalytic activity. Therefore, the clearly enhanced visible photocatalytic activity of CQDs/TiO_2 should not only be credited of the MB influence on TiO_2, but also to the function of CQDs. A comparison between present results and previous studies about the performance of dye removal by CQDs composites are displayed in Table 3.

Table 3: Comparison of photocatalytic degradation of methyl blue (MB) dye using CQDs-composites as photocatalyst

Photocatalyst	Optimum dose of catalyst	Concentration of MB	Degradation (%)	Visible Light Source	Time (min)	References
CQDs	100 mg/L	5 mg/L	73%	500 W halogen lamp	120	**This study**
TiO_2			27%			
CQDs-TiO_2			55%			
N-CQDs	100 mg/L	10 mg/L	80.1%	42 W LED panel	420	(Zhang et al., 2016)
TiO_2			53.8%			
N-CQDs-TiO_2			86.9%			
N-CQDs	20 mg/L	20 mg/L	100%	500 W halogen lamp	260	(Aghamali et al., 2018)
TNTs	10 mg/L	30 mg/L	45.6%	500 W xenon lamp	50	(Zhao et al., 2018)
CQDs/TNTs			91.3%			
CQDs	4 mL/L	45 µmol/L	~99.5%	60 W tungsten lamp	130	(Das et al., 2019)
N-CQDs	100 mL/L	10 mg/L	97 %	Sunlight	180	(Rani et al., 2021)
$SrTiO_3$	1500 mg/L	5 mg/L	0%	250 W halide lamp	200	(Cui et al., 2022)
Graphene			11%			
CQDs/$SrTiO_3$/ graphene			94%			

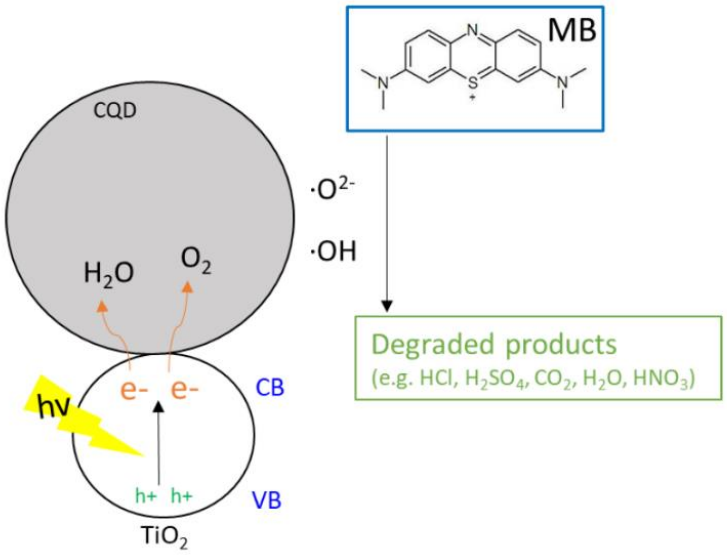

Figure 11: Possible degradation mechanism of MB with CQDs/TiO_2 composite.

4. Conclusion

The performance of CQDs, TiO_2, and CQDs/TiO_2 photocatalysts for MB dye degradation were studied by varying three parameters such as effect of catalyst loading, initial concentration of dye and pH. CQDs showed higher degradation percentage than TiO_2 and CQDs/TiO_2 throughout the range of initial concentration of MB considered. This finding was concurred to the porous characteristics obtained where CQDs was detected with the highest BET surface area and pore volume than the other catalysts, indicating CQDs has abundant active sites for effective degradation of MB. 0.1 g/L catalyst, 5 mg/L dye concentration and 9.00 pH offered the best photocatalytic degradation. CQDs possess the highest photo degradation (73%) of MB within 120 minutes via visible light irradiation compare to TiO_2 (55%) and CQDs/TiO_2 (27%) catalysts. Though we observed and addressed the dye removal rate only for 120 minutes but still there is a possibility to degreed more percentages of dye if we observe more time. That's why further research can be conducted to obtain and find the highest dye removal percentages. In summary, biomass derived CQDs can act as solely catalyst in degradation of dye simultaneously studies photocatalysts provides an insight for hydrogen evolution, CO_2 reduction, biomedical and biosensing application. The emerging of this finding is believed that the ability to reuse the water melon rinds (waste) while presenting an environmentally friendly solution for wastewater remediation.

Acknowledgements

Authors acknowledged the financial support provided by Universiti Malaysia Pahang (UMP) Postgraduate Research Scheme (PGRS220341).

Conflicts of Interest

The authors declare no conflict of interest.

References

Aghamali, A., Khosravi, M., Hamishehkar, H., Modirshahla, H., Behnajady, M.A., 2018. Synthesis and characterization of high efficient photoluminescent sunlight driven photocatalyst of N-Carbon Quantum Dots, J. Lumin., 201, Pp. 265–274. https://doi.org/10.1016/j.jlumin.2018.04.061.

Ahmad, K., Ghatak, H.R., Ahuja, S.M., 2020. A review on photocatalytic remediation of environmental pollutants and H2 production through water splitting: A sustainable approach, Environ. Technol. Innov., 19. https://doi.org/10.1016/j.eti.2020.100893.

Akpomie, K.G., Conradie, J., 2020. Advances in application of cotton-based adsorbents for heavy metals trapping, surface modifications and future perspectives, Ecotoxicol. Environ. Saf., 201, Pp. 110825. https://doi.org/10.1016/j.ecoenv.2020.110825.

Al-Tohamy, R., Ali, S.S., Li, F., Okasha, K.M., Mahmoud, Y.A.G., Elsamahy, T., Jiao, H., Fu, Y., Sun, J., 2022. A critical review on the treatment of dye-containing wastewater: Ecotoxicological and health concerns of textile dyes and possible remediation approaches for environmental safety, Ecotoxicol. Environ. Saf., 231, Pp. 113160. https://doi.org/10.1016/j.ecoenv.2021.113160.

Cui, J., Liu, J., Xia, X., Chai, X., Guo, H., Gao, J., Gao, S., 2022. Carbonized propagation synthesis of porous CQDs-SrTiO3/graphene and its photocatalytic performance for removal of methylene blue, Environ. Sci. Water Res. Technol., 8, Pp. 671–685. https://doi.org/10.1039/d1ew00758k.

Das, G.S., Shim, J.P., Bhatnagar, A., Tripathi, K.M., Kim, T.Y., 2019. Biomass-derived Carbon Quantum Dots for Visible-Light-Induced Photocatalysis and Label-Free Detection of Fe(III) and Ascorbic acid, Sci. Rep., 9, Pp. 1–9. https://doi.org/10.1038/s41598-019-49266-y.

Elsayed, M.H., Jayakumar, J., Abdellah, M., Mansoure, T.H., Zheng, K., Elewa, A.M., Chang, C.L., Ting, L.Y., Lin, W.C., hua Yu, H., Wang, W.H., Chung, C.C., Chou, H.H., 2021. Visible-light-driven hydrogen evolution using nitrogen-doped carbon quantum dot-implanted polymer dots as metal-free photocatalysts, Appl. Catal. B Environ., 283, Pp. 119659. https://doi.org/10.1016/j.apcatb.2020.119659.

Fan, H., Zhang, M., Bhandari, B., hui Yang, C., 2020. Food waste as a carbon source in carbon quantum dots technology and their applications in food safety detection. Trends Food Sci. Technol., 95, Pp. 86–96. https://doi.org/10.1016/j.tifs.2019.11.008.

Haque, F.Z., Nandanwar, R., Singh, P., 2017. Optik Evaluating photodegradation properties of anatase and rutile TiO 2 nanoparticles for organic compounds, Opt. - Int. J. Light Electron Opt., 128, Pp. 191–200. https://doi.org/10.1016/j.ijleo.2016.10.025.

Hou, C., Zou, Y., Wang, H., Wang, X., Xu, Y., Wang, Q., He, Z., Fan, J., Shi, L., Xu, L., Lin, F., Fang, D., 2019. Tailoring strain and lattice relaxation characteristics in InGaAs / GaAsP multiple quantum wells structure with phosphorus doping engineering, 770. https://doi.org/10.1016/j.jallcom.2018.08.119.

Jain, K., Patel, A.S., Pardhi, V.P., Flora, S.J.S., 2021. Nanotechnology in wastewater management: A new paradigm towards wastewater treatment, Molecules, 26. https://doi.org/10.3390/molecules26061797.

Jawad, A.H., Ngoh, Y.S., Radzun, K.A., 2018. Utilization of watermelon (Citrullus lanatus) rinds as a natural low-cost biosorbent for adsorption of methylene blue : kinetic , equilibrium and thermodynamic studies thermodynamic studies, J. Taibah Univ. Sci., Pp. 1–11. https://doi.org/10.1080/16583655.2018.1476206.

Jiaqi, Z., Yimin, D., Danyang, L., Shengyun, W., Liling, Z., Yi, Z., 2019. Synthesis of carboxyl-functionalized magnetic nanoparticle for the removal of methylene blue, Colloids Surfaces A., 572, Pp. 58–66. https://doi.org/10.1016/j.colsurfa.2019.03.095.

Juliet, S.S., Ramalingom, S., Ravidhas, C., Raj, A.M.E., 2017. Effect of Calcination Temperature on Titanium Oxide Nano crystallites in the Anatase Phase Synthesized by Sol-Gel Route, 9, Pp. 32–39. https://doi.org/10.9790/4861-0904043239.

Ke, J., Li, X., Zhao, Q., Liu, B., Liu, S., Wang, S., 2019. Journal of Colloid and Interface Science Upconversion carbon quantum dots as visible light responsive component for efficient enhancement of photocatalytic performance, J. Colloid Interface Sci., 496, Pp. 425–433. https://doi.org/10.1016/j.jcis.2017.01.121.

Khan, M.E., Mohammad, A., Yoon, T., 2022. State-of-the-art developments in carbon quantum dots (CQDs): Photo-catalysis, bio-imaging, and bio-sensing applications, Chemosphere, 302, Pp. 134815. https://doi.org/10.1016/j.chemosphere.2022.134815.

Kishor, R., Purchase, D., Saratale, G.D., Saratale, S.G., Ferreira, L.F.R., Bilal, M., Chandra, R., Bharagava, R.N., 2021. Ecotoxicological and health concerns of persistent coloring pollutants of textile industry wastewater and treatment approaches for environmental safety, J. Environ. Chem. Eng., 9, Pp. 105012. https://doi.org/10.1016/j.jece.2020.105012.

Kumar, A., Ray, A., Laha, D., Kumar, T., Karmakar, P., Kumar, S., 2017. Sensors and Actuators B : Chemical Green synthesis of carbon dots from Ocimum sanctum for effective fluorescent sensing of Pb 2 + ions and live cell imaging, Sensors Actuators B. Chem., 242, Pp. 679–686. https://doi.org/10.1016/j.snb.2016.11.109.

Kurian, M., 2021. Advanced oxidation processes and nanomaterials -a review, Clean. Eng. Technol., 2. https://doi.org/10.1016/j.clet.2021.100090.

Lima, H.H.C., Maniezzo, R.S., Llop, M.E.G., Kupfer, V.L., Arroyo, P.A., Guilherme, M.R., Rubira, A.F., Girotto, E.M., Rinaldi, A.W., 2019. Synthesis and characterization of pecan nutshell-based adsorbent with high speci fi c area and high methylene blue adsorption capacity, J. Mol. Liq., 276, Pp. 570–576. https://doi.org/10.1016/j.molliq.2018.12.010.

Liu, Q., 2020. Pollution and Treatment of Dye Waste-Water, in: IOP Conf. Ser. Earth Environ. Sci., IOP Publishing Ltd. https://doi.org/10.1088/1755-1315/514/5/052001.

Liu, Y., Liu, Y., Park, M., Park, S., Zhang, Y., Akanda, R., Park, B., Kim, H.Y., Green synthesis of fluorescent carbon dots from carrot juice for in vitro cellular imaging, 21, Pp. 61–67. https://doi.org/10.5714/CL.2017.21.061.

Mohamed, H., Alsanea, A.A., 2020. TiO 2 / carbon dots decorated reduced graphene oxide composites from waste car bumper and TiO 2 nanoparticles for photocatalytic applications, Arab. J. Chem., 13, Pp. 3082–3091. https://doi.org/10.1016/j.arabjc.2018.08.016.

Mudhoo, A., Ramasamy, D.L., Bhatnagar, A., Usman, M., Sillanpää, M., 2020. An analysis of the versatility and effectiveness of composts for sequestering heavy metal ions, dyes and xenobiotics from soils and aqueous milieus, Ecotoxicol. Environ. Saf., 197, Pp. 110587. https://doi.org/10.1016/j.ecoenv.2020.110587.

Olatunji, O.O., Estimation of the Elemental Composition of Biomass Using Hybrid Adaptive Neuro-Fuzzy Inference System.

Oyeniran, D.O., Sogbanmu, T.O., Adesalu, T.A., 2021. Antibiotics, algal evaluations and subacute effects of abattoir wastewater on liver function enzymes, genetic and haematologic biomarkers in the freshwater fish, Clarias gariepinus, Ecotoxicol. Environ. Saf., 212, Pp. 111982. https://doi.org/10.1016/j.ecoenv.2021.111982.

Phang, S.J., Tan, L.L., 2019. Recent advances in carbon quantum dot (CQD)-based two dimensional materials for photocatalytic applications, Catal. Sci. Technol., 9, Pp. 5882–5905. https://doi.org/10.1039/c9cy01452g.

Rani, U.A., Ng, L.Y., Ng, C.Y., Mahmoudi, E., 2020. A review of carbon quantum dots and their applications in wastewater treatment, Adv. Colloid Interface Sci. 278, Pp. 102124. https://doi.org/10.1016/j.cis.2020.102124.

Rani, U.A., Ng, L.Y., Ng, C.Y., Mahmoudi, E., Ng, Y.S., Mohammad, A.W., 2021. Sustainable production of nitrogen-doped carbon quantum dots for photocatalytic degradation of methylene blue and malachite green, J. Water Process Eng., 40, Pp. 101816. https://doi.org/10.1016/j.jwpe.2020.101816.

Samsami, S., Mohamadi, M., Sarrafzadeh, M.H., Rene, E.R., Firoozbahr, M., 2020. Recent advances in the treatment of dye-containing wastewater from textile industries: Overview and perspectives, Process Saf. Environ. Prot., 143, Pp. 138–163. https://doi.org/10.1016/j.psep.2020.05.034.

Shafique, M., Mahr, M.S., Yaseen, M., Bhatti, H.M., 2022. CQD/TiO2 nanocomposite photocatalyst for efficient visible light-driven purification of wastewater containing methyl orange dye, Mater. Chem. Phys., 278, Pp. 125583. https://doi.org/10.1016/j.matchemphys.2021.125583.

Shalahuddin Al Ja'farawy, M., Kusumandari, Purwanto, A., Widiyandari, H., 2022. Carbon quantum dots supported zinc oxide (ZnO/CQDs) efficient photocatalyst for organic pollutant degradation – A systematic review, Environ. Nanotechnology, Monit. Manag., 18, Pp. 100681. https://doi.org/10.1016/j.enmm.2022.100681.

Singh, M., Goyal, M., Devlal, K., 2018. Size and shape effects on the band gap of semiconductor compound nanomaterials, J. Taibah Univ. Sci., Pp. 1–6. https://doi.org/10.1080/16583655.2018.1473946.

Sugapriya, S., Sriram, R., Lakshmi, S., 2013. Optik Effect of annealing on TiO 2 nanoparticles, 124, Pp. 4971–4975. https://doi.org/10.1016/j.ijleo.2013.03.040.

Tharaneedhar, V., Kumar, P.S., Saravanan, A., Ravikumar, C., Jaikumar, V., 2017. Prediction and interpretation of adsorption parameters for the sequestration of methylene blue dye from aqueous solution using microwave assisted corncob activated carbon, Sustain. Mater. Technol. 11., Pp. 1–11. https://doi.org/10.1016/j.susmat.2016.11.001.

Titchou, F.E., Zazou, H., Afanga, H., El Gaayda, J., Ait Akbour, R., Nidheesh, P.V., Hamdani, M., 2021. Removal of organic pollutants from wastewater by advanced oxidation processes and its combination with membrane processes, Chem. Eng. Process. - Process Intensif., 169. https://doi.org/10.1016/j.cep.2021.108631.

Valencia, S., Marín, J.M., Restrepo, G., 2010. Study of the bandgap of synthesized titanium dioxide nanoparticules using the sol-gel method and a hydrothermal treatment, Open Mater. Sci. J., 4, Pp. 9–14. https://doi.org/10.2174/1874088X01004020009.

Wang, G., Xu, L., Zhang, J., Yin, T., Han, D., 2012. Enhanced Photocatalytic Activity of TiO 2 Powders (P25) via Calcination Treatment. https://doi.org/10.1155/2012/265760.

Wang, Y., Hu, A., 2014. Carbon quantum dots : synthesis , properties and applications, J. Mater. Chem. C Mater. Opt. Electron. Devices., 2, Pp. 6921–6939. https://doi.org/10.1039/C4TC00988F.

Yan, Y., Kuang, W., Shi, L., Ye, X., Yang, Y., Xie, X., Shi, Q., Tan, S., 2019. Carbon quantum dot-decorated TiO 2 for fast and sustainable antibacterial properties under visible-light, J. Alloys Compd., 777, Pp. 234–243. https://doi.org/10.1016/j.jallcom.2018.10.191.

Zhang, J., Zhang, X., Dong, S., Zhou, X., Dong, S., 2016. -doped carbon quantum dots/TiO2 hybrid composites with enhanced visible light driven photocatalytic activity toward dye wastewater degradation and mechanism insight, J. Photochem. Photobiol. A Chem., 325, Pp. 104–110. https://doi.org/10.1016/j.jphotochem.2016.04.012.

Zhao, F., Rong, Y., Wan, J., Hu, Z., Peng, Z., Wang, B., 2018. High photocatalytic performance of carbon quantum dots/TNTs composites for enhanced photogenerated charges separation under visible light, Catal. Today, 315, Pp. 162–170. https://doi.org/10.1016/j.cattod.2018.02.019.